Somatostatin Receptor 1 Selective Analogues: 4. Three-Dimensional Consensus Structure by NMR

Christy Rani R. Grace,[†] Lukas Durrer,[†] Steven C. Koerber,[‡] Judit Erchegyi,[‡] Jean Claude Reubi,[§] Jean E. Rivier,*[,‡] and Roland Riek[†]

Structural Biology Laboratory, The Salk Institute for Biological Studies, 10010 North Torrey Pines Road, La Jolla, California 92037, The Clayton Foundation Laboratories for Peptide Biology, The Salk Institute for Biological Studies, 10010 North Torrey Pines Road, La Jolla, California 92037, and Division of Cell Biology and Experimental Cancer Research, Institute of Pathology, University of Berne, Berne, Switzerland

Received June 18, 2004

The three-dimensional NMR structures of six analogues of somatostatin (SRIF) are described. These analogues with the amino acid 4-(*N*-isopropyl)-aminomethylphenylalanine (IAmp) at position 9 exhibit potent and highly selective binding to human SRIF subtype 1 receptors (sst_1). The conformations reveal that the backbones of these analogues have a hairpin-like structure similar to the sst_2-subtype-selective analogues. This structure serves as a scaffold for retaining a unique arrangement of the side chains of D-Trp[8], IAmp[9], Phe[7], and Phe[11] or m-I-Tyr[11] (m-I-Tyr = mono-iodo-tyrosine). The conformational preferences and results from biological analyses of these analogues[1,2] allow a detailed study of the structure−activity relationship of SRIF. The proposed consensus pharmacophore of the sst_1-selective analogues requires a unique set of distances between an indole/2-naphthyl ring, an IAmp side chain, and two aromatic rings. This motif is necessary and sufficient to explain the binding affinities of all of the analogues studied and is distinct from the existing models suggested for sst_4 as well as sst_2/sst_5 selectivity.

Introduction

Somatostatin (somatotropin release inhibiting factor, SRIF, H-Ala[1]-Gly[2]-c[Cys[3]-Lys[4]-Asn[5]-Phe[6]-Phe[7]-Trp[8]-Lys[9]-Thr[10]-Phe[11]-Thr[12]-Ser[13]-Cys[14]]-OH), a cyclic tetradecapeptide, inhibits the release of several hormones including growth hormone (GH), glucagon, insulin, secretin, and gastrin.[3,4] It also plays a vital role in neurotransmission and neuromodulation[5,6] and has antiproliferative effects, regulating cell proliferation and differentiation. SRIF elicits its effects via high-affinity interactions with a family of five different receptors, sst_{1-5}. Sequence homology is 39−57% among the five subtypes, and each subtype is highly conserved across different species. The functional significance of the endogenous receptors in mediating the diverse effects of SRIF requires the availability of subtype-selective agonists and antagonists, and hence SRIF continues to be a target for the development of subtype-specific analogues.[7−11]

Since the discovery of SRIF, numerous peptide and nonpeptide analogues have been described. With the characterization of the five sst, analogues can be tested for their biological activity in terms of affinity and selectivity.[7−9,12−14] Early structure−activity relationship (SAR) studies using in vitro functional assays suggested a central involvement of the side chains of residues Trp[8]-Lys[9] for biological recognition.[15−17] Furthermore, extensive structural studies including NMR and X-ray diffraction[18] have been carried out to elucidate the pharmacophore and the consensus structural motif of analogues binding predominantly to sst_2/sst_5 and sst_4 receptors. According to the proposed model for sst_2/sst_5 binding,[19−22] the side chains and the relative spatial arrangement of Phe[7], D-Trp[8], and Lys[9] constitute the most essential elements (Figure 4D). The side chain of D-Trp[8] is in close proximity to the side chain of Lys[9] (∼4 Å), whereas the side chain of Phe[7] is about 7−9 Å away from the side chain of D-Trp[8] and 9−11 Å from the side chain of Lys[9]. Recently, our group studied the structures of sst_4-selective SRIF analogues from three different families by NMR in dimethyl sulfoxide (DMSO) and proposed a pharmacophore model for these analogues.[23] Although these analogues have different backbone conformations, the relative spatial arrangement of the side chains of D-Trp[8], Lys[9], and Phe[6] or Phe[11] were unique, and on this basis it was proposed that these residues and their observed proximity were important for binding. This binding motif mainly differs from the binding motif for sst_2/sst_5-selective receptors in the proximity of the side chains of Lys and Phe, which is 4.5−6.5 Å in the sst_4 and 9−11 Å in the sst_2/sst_5 binding motifs (Figure 4C and D). These studies furthermore strongly support the idea of Nicolaou et al., who suggested that the backbone is not required for receptor binding but serves as a scaffold for supporting the important side chains.[24]

In this paper, the studies of Grace et al.[23] on the characterization of the sst_4 pharmacophore and of Falb et al.[20] on the sst_2 pharmacophore have been further extended to propose a pharmacophore model for sst_1-selective analogues. In the preceding two papers, the synthesis and biological characterization of two families of structurally constrained sst_1-selective SRIF analogues

* Author to whom correspondence should be addressed. Phone: (858) 453-4100. Fax: (858) 552-1546. E-mail: jrivier@salk.edu.

[†] Structural Biology Laboratory, The Salk Institute for Biological Sciences.

[‡] The Clayton Foundation Laboratories for Peptide Biology, The Salk Institute for Biological Sciences.

[§] Division of Cell Biology and Experimental Cancer Research, Institute of Pathology, University of Berne.

10.1021/jm049518u CCC: $30.25
Published on Web 12/23/2004

are described.[1,2] Six analogues from these families, which bind selectively to the sst_1 receptor, have been studied by NMR (Table 1). These analogues differ as follows: **1** has a lactam bridge from Glu^6 to Lys^{12}, **2** has a lactam bridge from Glu^7 to $Dbu(\beta Ala)^{12}$, **3** and **4** are the same as **2** but contain Lys or L-hhLys in the bridging position 12 (Dbu(βAla) = diaminobutyric acid, βAla = $H_2N-CH_2-CH_2-COOH$, L-hhLys = L-2,8-diaminooctanoic acid = L-homo-homo-lysine). Analogues **5** and **6** lack residue Tyr^2 and the lactam bridge, and they differ from each other at position 7 by Phe and Ala, respectively. All of the analogues are cyclic with the disulfide bridge between Cys^3 and Cys^{14}. Although all of these analogues bind selectively to the sst_1 receptor, their binding affinities vary from 200 nM for **1** to 2.5 nM for **5**.

Results

In this section, the chemical shift assignment and the structure determination by NMR of each SRIF analogue **1**−**6** given in Table 1 are presented. These six sst_1-selective analogues were selected to cover the chemical diversity uncovered in the two preceding papers[1,2] and judged necessary and sufficient to elucidate the corresponding pharmacophore.

Chemical Shift Assignment, Collection of Structural Restraints, and Structure Determination. The nearly complete chemical shift assignment of proton resonances (Supporting Information) for **1**−**6** (Table 1) has been carried out using two-dimensional (2D) NMR experiments using the standard procedure described in the Experimental Section. The N-terminal amino protons for **1** to **4** were not observed due to fast exchange with the solvent. Furthermore, some aromatic ring protons could not be assigned as shown in the Supporting Information. Due to the presence of the carbamoyl group at the N-terminus for analogues **5** and **6**, the (Cbm) amide proton of Cys^3 is observed at high field. For all six analogues, the nuclear Overhauser enhancement spectroscopy (NOESY) spectrum was measured with a mixing time of 100 ms, leading to approximately 150 meaningful distance restraints per analogue (Table 2). The NOEs observed were indicative of hairpinlike structures in all of the six analogues. The $^3J_{HN\alpha}$ coupling constants could not be derived from the one-dimensional (1D) spectra due to line broadening and peak overlap observed in the amide region of the spectrum. These NOE distance restraints were used as input for the structure calculation with the program CYANA[25] followed by restrained energy minimization using the program DISCOVER[26] (for more details see the Experimental Section). The resulting bundle of 20 conformers per analogue represents the three-dimensional (3D) solution structure of each analogue. For each analogue, the small residual constraint violations in the 20 refined conformers (Table 2) and the good coincidence of experimental NOEs and short interatomic distances (data not shown) indicate that the input data represent a self-consistent set and that the restraints are well-satisfied in the calculated conformers (Table 2). The deviations from ideal geometry are minimal, and similar energy values were obtained for all 20 conformers of each analogue (Figure 2). The root-mean-square deviation (rmsd) obtained for the sst_1-selective analogues is

Table 1. Sst_{1-5} Binding Affinities of Analogues Studied by NMR[a]

ID	analogue	IC_{50} (nM) sst_1	sst_2	sst_3	sst_4	sst_5
1	dicyclo(3−14, 6−12)H-Tyr-Cys^3-Lys-Glu^6-Phe-D-Trp-IAmp-Thr-Phe-Lys^{12}-Ser-Cys^{14}-OH	208 (250,166)	> 1K (2)	> 1K (2)	> 1K (2)	> 1K (2)
2	dicyclo(3−14, 7−12)H-Tyr-Cys^3-Lys-Phe-Glu^7-D-Trp-IAmp-Thr-Phe-$Dbu(\beta Ala)^{12}$-Ser-Cys^{14}-OH	74 ± 22 (3)	> 1K (3)	> 1K (3)	> 1K (3)	> 1K (3)
3	dicyclo(3−14, 7−12)H-Tyr-Cys^3-Lys-Phe-Glu^7-D-Trp-IAmp-Thr-Phe-Lys^{12}-Ser-Cys^{14}-OH	53 ± 18 (3)	> 1K (3)	> 1K (3)	> 1K (3)	> 1K (3)
4	dicyclo(3−14, 7−12)H-Tyr-Cys^3-Lys-Phe-Glu^7-D-Trp-IAmp-Thr-Phe-L-$hhLys^{12}$-Ser-Cys^{14}-OH	16 ± 6 (4)	> 1K (4)	> 1K (4)	> 1K (4)	> 1K (4)
5	cyclo(3−14)Cbm-Cys^3-Lys-Phe-Phe-D-Trp-IAmp-Thr-m-I-Tyr-Thr-Ser-Cys^{14}-OH	2.5 ± 0.2 (4)	> 1K (4)	618 ± 125 (4)	> 1K (4)	> 1K (4)
6	cyclo(3−14)Cbm-Cys^3-Lys-Phe-Ala-D-Trp-IAmp-Thr-m-I-Tyr-Thr-Ser-Cys^{14}-OH	98 (64 ± 132)	> 1K (2)	> 1K (2)	> 1K (2)	> 1K (2)
7	cyclo(3−14)[H-Cys^3-Phe-Phe-Trp-Lys-Thr-Phe-Cys^{14}-OH (analogue **1** in Grace et al.[23])	5.3 ± 0.7 (3)	130 ± 65 (3)	13 ± 0.7 (3)	0.7 ± 0.3 (3)	14 ± 4.1 (3)

[a] The data are obtained from refs 1, 2, 7−9.

Table 2. Characterization of the NMR Structures of Analogues **1**-**6**[a]

ID	NOE distance restraints[b]	angle restraints	CYANA target function[c]	backbone rmsd (Å)	overall rmsd (Å)	CFF91 energies (kcal/mol)			residual restraint violations on			
									distances		dihedral angles	
						total energy	van der Waals	electrostatic	no. ≥ 0.1 Å	max (Å)	no. ≥ 1.5 deg	max (deg)
1	231	29	0.39	0.41 ± 0.10	1.12 ± 0.17	139.3 ± 8.0	10.1 ± 6.4	94.6 ± 3.0	0.9 ± 0.2	0.10 ± 0.02	0.1 ± 0.2	0.06 ± 0.22
2	137	28	0.34	1.04 ± 0.48	2.36 ± 0.61	88.3 ± 11.5	39.3 ± 4.1	33.9 ± 9.0	0.7 ± 0.4	0.13 ± 0.08	0.4 ± 0.9	0.41 ± 0.86
3	166	23	0.27	1.27 ± 0.21	2.20 ± 0.39	154.6 ± 7.5	46.3 ± 5.7	86.8 ± 7.4	0.3 ± 0.1	0.09 ± 0.04	0	0
4	135	25	0.38	0.54 ± 0.18	1.66 ± 0.34	160.0 ± 12.5	41.3 ± 4.8	104.0 ± 6.7	1.0 ± 0.1	0.26 ± 0.03	0.2 ± 0.7	0.21 ± 0.62
5	151	36	0.35	1.11 ± 0.34	1.85 ± 0.55	172.3 ± 9.3	41.4 ± 4.5	115.5 ± 6.5	1.1 ± 0.2	0.16 ± 0.03	0.1 ± 0.3	0.07 ± 0.31
6	176	25	0.56	0.95 ± 0.46	1.58 ± 0.41	201.8 ± 9.5	39.8 ± 4.2	126.7 ± 5.9	2.1 ± 0.4	0.19 ± 0.04	0	0

[a] The bundle of 20 conformers with the lowest residual target function was used to represent the NMR structures of each analogue. [b] Meaningful NOE distance restraints include intraresidual and sequential NOEs.[25] [c] The target function is zero only if all the experimental distance and torsion angle constraints are fulfilled and all nonbonded atom pairs satisfy a check for the absence of steric overlap. The target function is proportional to the sum of the square of the difference between calculated distance and isolated constraint or van der Waals restraints and similarly isolated angular restraints are included in the target function. For the exact definition see ref 25.

higher than that for the sst_4-selective analogues, recently published by our group. This can be explained by the smaller number of experimental NOEs per residue observed than those for the sst_4-selective analogues, where an exceptionally large number of NOEs was observed and documented.[23] To describe the 3D structures of **1** to **6** in a simple manner, we introduce the term "front side", which is defined as the surface of the peptide facing the reader when the peptide is oriented with the C-terminus on the left. The opposite surface of the peptide is correspondingly named the "backside".

Three-Dimensional Structure of Dicyclo(3−14, 6−12)H-Tyr^2-Cys^3-Lys^4-Glu^6-Phe^7-D-Trp^8-IAmp^9-Thr^{10}-Phe^{11}-Lys^{12}-Ser^{13}-Cys^{14}-OH (1). Analogue **1** binds to the sst_1 receptor with low affinity (IC_{50} = 200 nM) and does not bind to the other receptors. The quality of the structure is reflected by the small backbone rmsd (Table 2), which can also be visually discerned from Figure 2 showing the bundle of 20 conformers representing the 3D structure. On the basis of the backbone torsion angles (Table 3), the 3D structure contains a β-turn of type-IV around D-Trp^8-IAmp^9, which is supported by the sequential and medium-range backbone NOE $\{d_{\alpha N}(i,i+2)\}$ between D-Trp^8 and Thr^{10} (Figure 1). Strong sequential $d_{\alpha N}(i,i+1)$ and the weak $d_{NN}(i,i+1)$ NOEs further confirm β-sheet structure of the analogue. The structure is further stabilized as evidenced by the presence of a few long-range NOEs, $d_{\alpha\alpha}(3,14)$, $d_{\alpha\beta}(4,3)$, $d_{N\alpha}(4,14)$, $d_{\alpha\alpha}(6,12)$, and $d_{\alpha N}(6,13)$. The low-temperature coefficient of −1.4 ppb/K experimentally observed for the amide proton of Thr^{10} is indicative of the observed hydrogen bond Thr^{10}NH−O′Glu^6. From the torsion angles listed in Table 3, it can be easily seen that the side chains of Phe^7 and Phe^{11} are in the gauche$^-$ rotamer and that of D-Trp^8 and IAmp^9 are in the gauche$^+$ rotamer. Concomitantly, the side chains of D-Trp^8 and IAmp^9 are oriented adjacent to each other, at the end of the hairpin pointing to the "front side", whereas the aromatic rings of Phe^7 and Phe^{11} are oriented adjacent to each other, at the "backside" of the peptide. The lactam bridge is on the "front side" (Figures 2 and 3).

Three-Dimensional Structure of Dicyclo(3−14, 7−12)H-Tyr^2-Cys^3-Lys^4-Phe^6-Glu^7-D-Trp^8-IAmp^9-Thr^{10}-Phe^{11}-Dbu(βAla)^{12}-Ser^{13}-Cys^{14}-OH (2). Analogue **2** has a slightly higher binding affinity to sst_1 than **1**. It differs from **1** only in the position of the lactam bridge between Glu^7 and Dbu(βAla)^{12}, which has a longer side chain than the Lys^{12} of **1**. The different position of the bridge orients the aromatic side chains differently and gives the backbone more flexibility (Figures 2 and 3). The strong sequential $d_{\alpha N}(i,i+1)$ and the weak $d_{NN}(i,i+1)$ NOEs as well as the long range $d_{\alpha\alpha}(3,14)$, $d_{N\alpha}(4,14)$, $d_{NN}(7,10)$, and $d_{NN}(8,11)$ NOEs further confirm a β-sheet structure. The backbone torsion angles (Table 3) indicate that the 3D structure contains a β-turn of type-II′ around D-Trp^8-IAmp^9, which was stabilized by the presence of the hydrogen bond between the amide proton of Thr^{10} and the carbonyl of Glu^7. The low-temperature coefficient of −0.3 ppb/K experimentally observed for the amide proton of Thr^{10} is indicative of the expected hydrogen bond Thr^{10}NH−O′Glu^7. It can be seen from the torsion angles that the

Table 3. Torsion Angles ϕ, ψ, and χ_1 (in degrees) of the Bundle of 20 Energy Minimized Conformers

ID	angle	Cys^3	Lys^4	Glu^6	Phe^7	D-Trp^8	IAmp^9	Thr^{10}	Phe^{11}	Lys^{12}	Ser^{13}	Cys^{14}
1	ϕ	-117 ± 12	-126 ± 26	-76 ± 9	34 ± 53	-75 ± 1	62 ± 4	-137 ± 7	-42 ± 23	-99 ± 10	-77 ± 8	-120 ± 37
	ψ	-167 ± 2	113 ± 10	-9 ± 75	-131 ± 3	38 ± 11	63 ± 2	-143 ± 5	135 ± 8	115 ± 7	100 ± 18	
	χ_1	-57 ± 6	46 ± 52	-44 ± 12	-29 ± 4	49 ± 1	-66 ± 4	-176 ± 2	124 ± 56	-84 ± 28	-174 ± 29	-114 ± 54
ID	angle	Cys^3	Lys^4	Phe^6	Glu^7	D-Trp^8	IAmp^9	Thr^{10}	Phe^{11}	Dbu^{12}	Ser^{13}	Cys^{14}
2	ϕ	-99 ± 67	-124 ± 31	-133 ± 30	-123 ± 12	112 ± 28	-59 ± 64	-105 ± 41	-73 ± 26	-141 ± 27	148 ± 65	65 ± 59
	ψ	123 ± 21	125 ± 17	137 ± 9	23 ± 26	-112 ± 8	0 ± 24	40 ± 23	114 ± 20	90 ± 55	-165 ± 23	
	χ_1	-85 ± 42	-81 ± 68	26 ± 61	-79 ± 37	-120 ± 84	4 ± 56	-61 ± 10	179 ± 9	51 ± 44	74 ± 7	-162 ± 15
ID	angle	Cys^3	Lys^4	Phe^6	Glu^7	D-Trp^8	IAmp^9	Thr^{10}	Phe^{11}	Lys^{12}	Ser^{13}	Cys^{14}
3	ϕ	-103 ± 82	-1 ± 94	81 ± 48	-110 ± 9	136 ± 13	-77 ± 14	-174 ± 4	-49 ± 11	-140 ± 22	-101 ± 92	-53 ± 79
	ψ	-92 ± 75	124 ± 46	89 ± 8	-2 ± 10	-56 ± 13	-58 ± 6	174 ± 6	94 ± 13	113 ± 30	153 ± 74	
	χ_1	-42 ± 70	-69 ± 72	-121 ± 61	68 ± 56	39 ± 13	164 ± 85	-138 ± 5	12 ± 93	40 ± 78	108 ± 98	-42 ± 73
ID	angle	Cys^3	Lys^4	Phe^6	Glu^7	D-Trp^8	IAmp^9	Thr^{10}	Phe^{11}	L-hhLys^{12}	Ser^{13}	Cys^{14}
4	ϕ	-87 ± 19	71 ± 51	-72 ± 24	125 ± 46	-62 ± 8	-95 ± 30	-73 ± 11	-151 ± 12	-64 ± 16	-16 ± 63	-15 ± 58
	ψ	-73 ± 25	113 ± 38	-69 ± 23	174 ± 11	-70 ± 14	-41 ± 9	175 ± 12	33 ± 2	19 ± 61	130 ± 48	
	χ_1	-93 ± 19	-115 ± 90	-86 ± 11	-113 ± 12	47 ± 27	51 ± 41	26 ± 9	-123 ± 7	-76 ± 73	-90 ± 105	13 ± 65
ID	angle	Cys^3	Lys^4	Phe^6	Phe^7	D-Trp^8	IAmp^9	Thr^{10}	m-I-Tyr^{11}	Thr^{12}	Ser^{13}	Cys^{14}
5	ϕ		-145 ± 71	-71 ± 48	-115 ± 59	65 ± 9	59 ± 2	-151 ± 6	-48 ± 10	-117 ± 49	-131 ± 62	-79 ± 64
	ψ	-158 ± 5	65 ± 16	-32 ± 30	-171 ± 11	180 ± 4	-79 ± 6	-152 ± 8	162 ± 35	161 ± 20	-47 ± 88	
	χ_1	-65 ± 61	-104 ± 23	165 ± 68	-37 ± 82	73 ± 4	167 ± 8	-171 ± 25	-68 ± 55	84 ± 39	-170 ± 71	-143 ± 80
ID	angle	Cys^3	Lys^4	Phe^6	Ala^7	D-Trp^8	IAmp^9	Thr^{10}	m-I-Tyr^{11}	Thr^{12}	Ser^{13}	Cys^{14}
6	ϕ		156 ± 54	-73 ± 30	-177 ± 20	145 ± 12	-164 ± 20	-64 ± 8	-35 ± 19	-10 ± 55	-92 ± 27	-106 ± 67
	ψ	62 ± 5	148 ± 24	-69 ± 6	108 ± 23	-133 ± 24	-46 ± 4	-102 ± 15	-59 ± 25	180 ± 25	-48 ± 16	
	χ_1	-162 ± 17	-133 ± 67	-116 ± 4	176 ± 20	0 ± 21	66 ± 12	-71 ± 10	18 ± 12	62 ± 13	-163 ± 8	91 ± 104

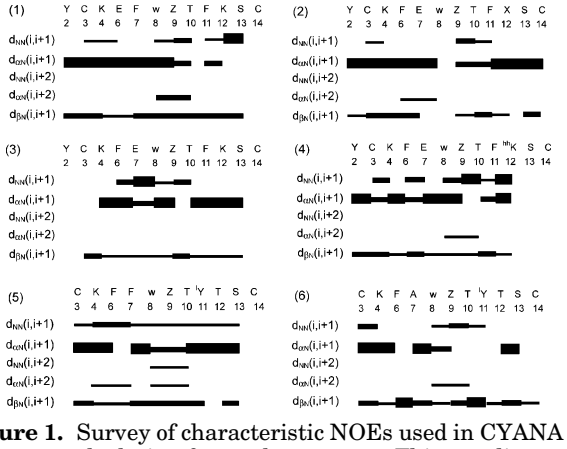

Figure 1. Survey of characteristic NOEs used in CYANA for structure calculation for analogues **1**−**6**. Thin, medium, and thick bars represent weak (4.5−6 Å), medium (3−4.5 Å), and strong (<3 Å) NOEs observed in the NOESY spectrum. The medium-range connectivities $d_{NN}(i,i+2)$ and $d_{\alpha N}(i,i+2)$ NOEs are shown by lines starting and ending at the positions of the residues related by the NOE. Residues designated with "w", "Z", "X", "^{hh}K", and "^{I}Y" correspond to the amino acids D-Trp, IAmp, Dbu(βAla), L-hhLys, and m-I-Tyr, respectively.

side chains of Glu^7, IAmp^9, and Thr^{10} are in the gauche$^+$ rotamer and that of D-Trp^8 and Phe^{11} are in the trans rotamer (Table 3). These rotamer positions result in a conformation in which the side chains of D-Trp^8 and IAmp^9 are adjacent to each other in the plane of the analogue backbone, whereas the side chains of Phe^6 and Phe^{11} are adjacent on the front side of the peptide backbone. The lactam bridge is on the backside of the peptide backbone, far away from D-Trp^8 and IAmp^9 (Figures 2 and 3).

Three-Dimensional Structure of Dicyclo(3−14, 7−12)H-Tyr^2-Cys^3-Lys^4-Phe^6-Glu^7-D-Trp^8-IAmp^9-Thr^{10}-Phe^{11}-Lys^{12}-Ser^{13}-Cys^{14}-OH (3). Analogue **3** differs from **2** at position 12 by Lys and has a similar binding affinity as **2**. The strong sequential $d_{\alpha N}(i,i+1)$ and the few $d_{NN}(i,i+1)$ NOEs, as well as the long range $d_{\alpha\alpha}(6,11)$, $d_{NN}(6,11)$, and $d_{NN}(7,10)$ NOEs, further confirm the β-turn structure. The calculated NMR structure has a type-II-like β-turn around D-Trp^8 and IAmp^9 (Figure 2 and Table 3) that has been stabilized by the observed hydrogen bond between the amide proton of Glu^7 and carbonyl of Thr^{10}. The temperature coefficient for Glu^7 (NH) could not be measured experimentally due to line broadening and overlap. From the observed torsion angles, it can be seen that the side chain of D-Trp^8 is in the gauche$^-$ rotamer, that of IAmp^9 is in the trans rotamer orientation, and the aromatic side chains at Phe^6 and Phe^{11} are adjacent in space and oriented on the front side of the peptide with the lactam bridge on the backside. The side chains of D-Trp^8 and IAmp^9 are pointing away from each other at the tip of the hairpinlike structure. The resulting close proximity between IAmp^9 and the side chain of Thr^{10} is supported by the upfield shift of the protons (Supporting Information). These upfield shifts are not observed in **2** due to different spatial arrangement of IAmp^9. The lactam bridge is close to the critical IAmp^9 side chain in **3** (Figure 3).

Three-Dimensional Structure of Dicyclo(3−14, 7−12)H-Tyr^2-Cys^3-Lys^4-Phe^6-Glu^7-D-Trp^8-IAmp^9-Thr^{10}-Phe^{11}-L-hhLys^{12}-Ser^{13}-Cys^{14}-OH (4). Analogue **4** differs from **2** and **3** at position 12 with L-hhLys instead of Dbu(βAla) and Lys, respectively. The longer side chain in **4** led to higher binding affinity compared to that of **2** and **3**.[2] The strong sequential $d_{\alpha N}(i,i+1)$ NOEs and the $d_{\alpha N}(i,i+2)$ NOE between D-Trp^8 and Thr^{10} confirm the type-III β-turn around D-Trp^8 and IAmp^9 (Figure 2 and Table 3). The structure is further stabilized as evidenced by the presence of some long range $d_{\alpha N}(3,14)$, $d_{\alpha N}(6,13)$, $d_{\alpha\alpha}(6,11)$, and $d_{\alpha N}(7,11)$ NOEs. Temperature coefficients could not be measured experimentally for the amide protons due to line broad-

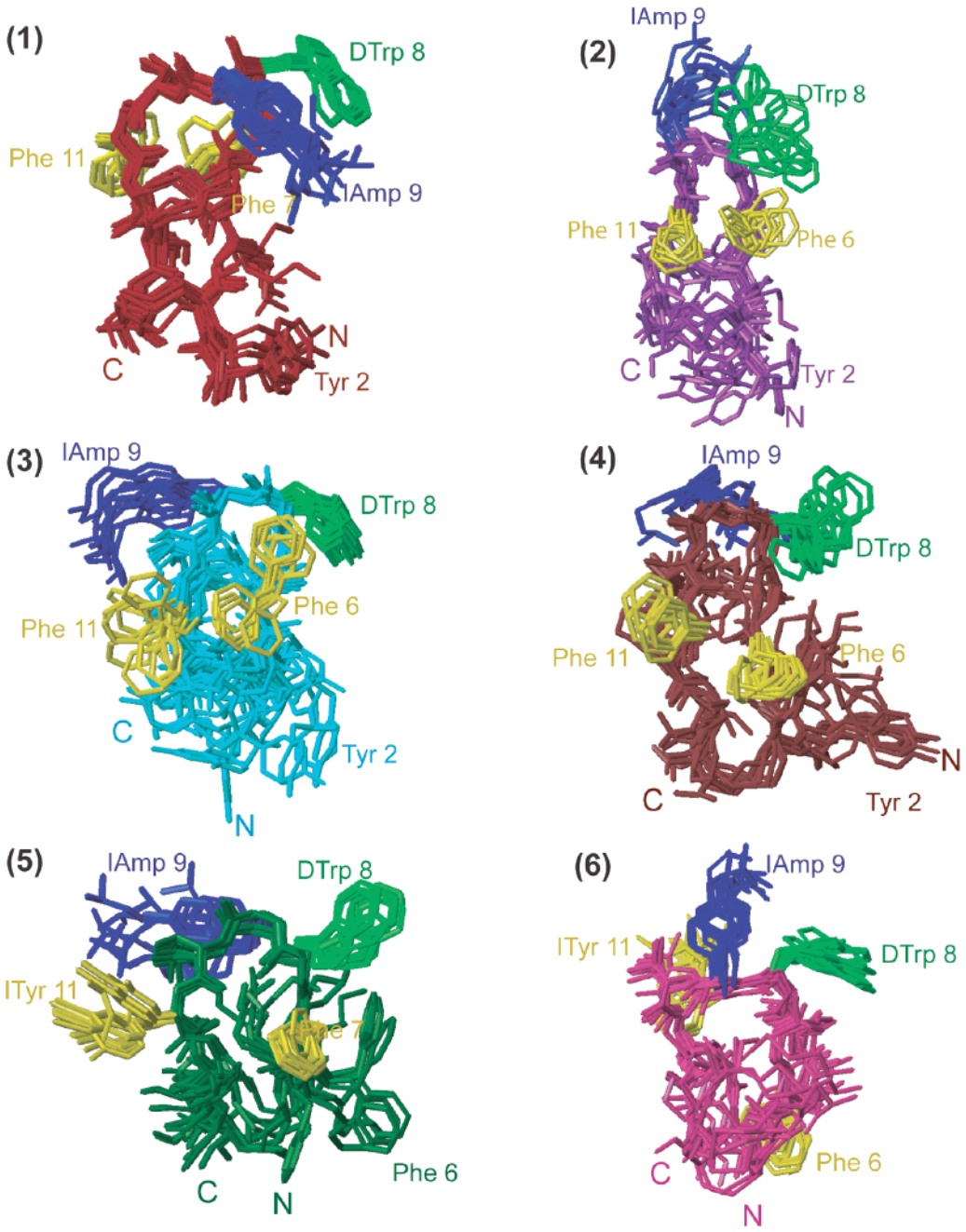

Figure 2. NMR structures of analogues **1**−**6**. For each analogue, 20 energy-minimized conformers with the lowest target function are used to represent the 3D NMR structure. The bundle is obtained by superposing the C^{α} atoms of the residues 2−10. The backbone and all side chains are displayed including the disulfide bridge as well as the lactam bridge. The peptides are oriented from C-terminus to the N-terminus and this surface of the peptide is referred to as the "front side" and the opposite side hidden on the paper is referred to as the "backside". The following color code is used: red (**1**) dicyclo(3−14, 6−12)H-Tyr-Cys^{3}-Lys-Glu^{6}-Phe-D-Trp-IAmp-Thr-Phe-Lys^{12}-Ser-Cys^{14}-OH; violet (**2**) dicyclo(3−14, 7−12)H-Tyr-Cys^{3}-Lys-Phe-Glu^{7}-D-Trp-IAmp-Thr-Phe-Dbu(βAla)^{12}-Ser-Cys^{14}-OH; cyan (**3**) dicyclo(3−14, 7−12)H-Tyr-Cys^{3}-Lys-Phe-Glu^{7}-D-Trp-IAmp-Thr-Phe-Lys^{12}-Ser-Cys^{14}-OH; brown (**4**) dicyclo(3−14, 7−12)H-Tyr-Cys^{3}-Lys-Phe-Glu^{7}-D-Trp-IAmp-Thr-Phe-L-hhLys^{12}-Ser-Cys^{14}-OH; dark green (**5**) cyclo(3−14)Cbm-Cys^{3}-Lys-Phe-Phe-D-Trp-IAmp-Thr-m-I-Tyr-Thr-Ser-Cys^{14}-OH; pink (**6**) cyclo(3−14)Cbm-Cys^{3}-Lys-Phe-Ala-D-Trp-IAmp-Thr-m-I-Tyr-Thr-Ser-Cys^{14}-OH. The residues involved in binding are colored the same in all the analogues, with IAmp (blue), D-Trp (light green), and Phe and m-I-Tyr (yellow).

ening and overlap problems. From the observed torsion angles, it can be seen that the side chains of D-Trp^{8} and IAmp^{9} are in the gauche^{-} rotamer, and the aromatic side chains of Phe^{6} and Phe^{11} are in the gauche^{+} rotamer orientation. This results in a conformation in which the aromatic side chains of Phe^{6} and Phe^{11} are oriented adjacent to each other on the front side with the lactam bridge on the backside of the peptide (Figures 2 and 3).

Three-Dimensional Structure of Cyclo(3−14)-Cbm-Cys^{3}-Lys^{4}-Phe^{6}-Phe^{7}-D-Trp^{8}-IAmp^{9}-Thr^{10}-m-I-Tyr^{11}-Thr^{12}-Ser^{13}-Cys^{14}-OH (5) (Cbm = Carbamoyl = H_2N-CO-). Analogue **5** binds with high affinity and selectively to the sst_1 receptor. The chemical structure differs from that of **1** to **4** by the carbamoylated N-terminus, m-I-Tyr at position 11, Thr at position 12, the absence of the lactam bridge, and the residue Tyr^{2}. These chemical modifications change the backbone from

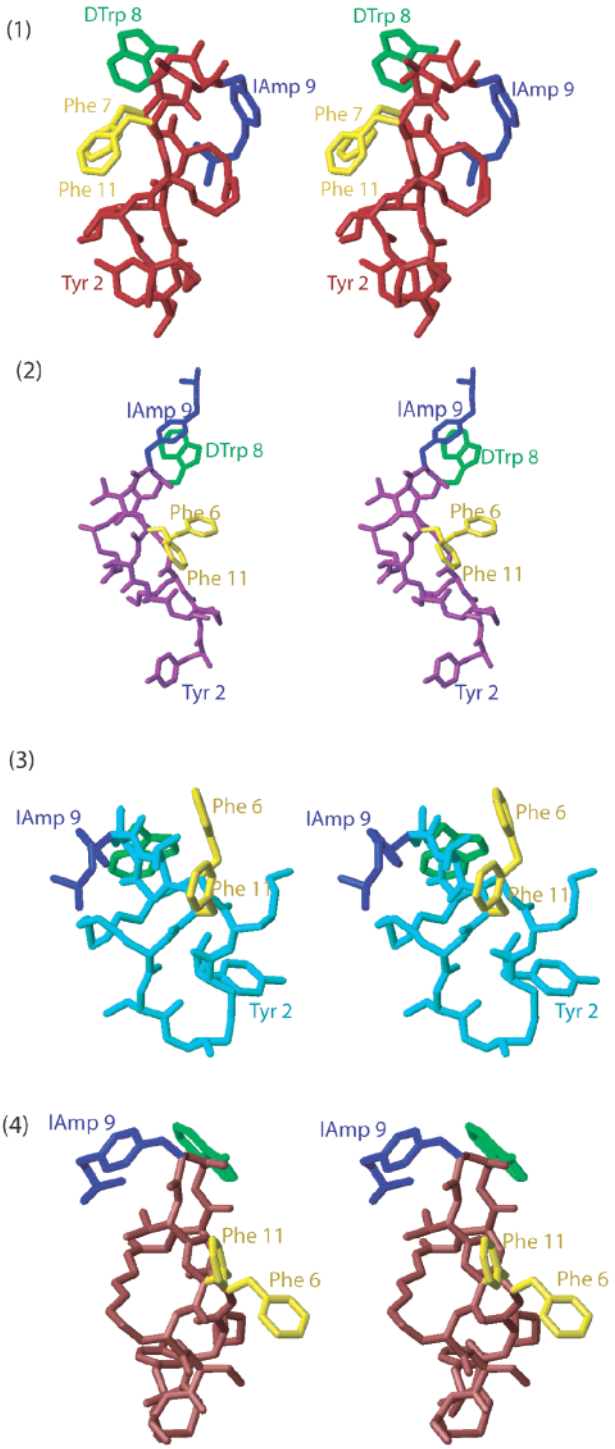

Figure 3. Stereoview of the structure of the analogues **1**−**4**, with the dicyclic bridges in the side view showing the orientation of the aromatic side chains with respect to the lactam bridge and the disulfide bridge. The following color code is used: red (**1**) dicyclo(3−14, 6−12)H-Tyr-Cys^{3}-Lys-Glu^{6}-Phe-D-Trp-IAmp-Thr-Phe-Lys^{12}-Ser-Cys^{14}-OH; violet (**2**) dicyclo(3−14, 7−12)H-Tyr-Cys^{3}-Lys-Phe-Glu^{7}-D-Trp-IAmp-Thr-Phe-Dbu(βAla)^{12}-Ser-Cys^{14}-OH; cyan (**3**) dicyclo(3−14, 7−12)H-Tyr-Cys^{3}-Lys-Phe-Glu^{7}-D-Trp-IAmp-Thr-Phe-Lys^{12}-Ser-Cys^{14}-OH; brown (**4**) dicyclo(3−14, 7−12)H-Tyr-Cys^{3}-Lys-Phe-Glu^{7}-D-Trp-IAmp-Thr-Phe-L-hhLys^{12}-Ser-Cys^{14}-OH. The residues involved in binding are colored as IAmp (blue), D-Trp (light green), and Phe (yellow). Analogue **1** has the aromatic side chains Phe^{7} and Phe^{11} oriented on the "backside" of the peptide, different from that of analogues **2** to **4**, where they are oriented on the "front side", with the lactam bridge on the "backside", which explains the lower binding affinity of **1**.

a β-turn to a γ-turn around IAmp^{9}, resulting in a different 3D structure. The γ-turn is supported by the weak $d_{\alpha N}(i,i+2)$ and $d_{NN}(i,i+2)$ NOEs between D-Trp^{8} and Thr^{10} and by the observed hydrogen bond D-Trp^{8}-HN−O′Thr^{10}. The low-temperature coefficient of −1.3 ppb/K measured experimentally for the amide hydrogen of D-Trp^{8} is further indicative of the hydrogen bond formation. On the basis of the torsion angles given in Table 3, it can be seen that the side chain of D-Trp^{8} is in the gauche^{-} rotamer, that of Phe^{6}, IAmp^{9}, and Thr^{10} are in the trans rotamer, and that of m-I-Tyr^{11} is in the gauche^{+} rotamer. Concomitantly, the side chains of D-Trp^{8} and IAmp^{9} are pointing away from each other, with the side chain of Phe^{7} close to the side chain of D-Trp^{8} in the front side (Figure 2). The close proximity is supported by the ring current, resulting in the upfield shift of the aromatic protons of Phe^{7}.

Three-Dimensional Structure of Cyclo(3−14)-Cbm-Cys^{3}-Lys^{4}-Phe^{6}-Ala^{7}-D-Trp^{8}-IAmp^{9}-Thr^{10}-m-I-Tyr^{11}-Thr^{12}-Ser^{13}-Cys^{14}-OH (6). Analogue **6** binds with moderate affinity and differs from **5** by the replacement of Phe^{7} by Ala^{7}. Originally, **6** was synthesized and analyzed in order to define the role of Phe^{6} in the binding affinity of **5**. The backbone in the calculated structure (Figure 2) is very different from that of **5** with a kink at IAmp^{9} and a type-III-like β-turn around Thr^{10} and m-I-Tyr^{11}, which is supported by the few strong $d_{\alpha N}(i,i+1)$ and weak $d_{NN}(i,i+1)$ observed (Figure 1). Furthermore, there were no long-range NOEs nor hydrogen bonds observed in all of the 20 calculated structures. On the basis of the side chain torsion angles, it can be seen that the side chains of Phe^{6} and Thr^{10} are in the gauche^{+} rotamer, Ala^{7} is in the trans rotamer, and IAmp^{9} is in the gauche^{-} rotamer (Table 3). This orients the side chains of Phe^{6} and m-I-Tyr^{11} to the backside of the peptide backbone as in the case of **1**.

Discussion

Our group has synthesized a large number of cyclic and dicyclic analogues of SRIF, some of which bind selectively with high affinity to the sst$_1$ receptor.[1,7] We have shown here that the understanding of the structural requirements of cyclic SRIF analogues binding to sst$_1$ receptor selectively, derived from extensive structural studies of two peptide families, can lead to the identification of the binding motif based on the 3D consensus structure. This, in turn, can be utilized in a predictive manner in designing selective SRIF analogues. The characterization of the bioactive conformation and the elucidation of the consensus 3D structural motif for the sst$_1$-selective SRIF analogues **1**−**6** (Table 1) are carried out using high-resolution NMR techniques. Assuming that the compounds studied in DMSO are in their bioactive conformation,[20,27] the proposed consensus structure is equivalent to the binding motif of sst$_1$-selective analogues and hence represents a pharmacophore for the sst$_1$ receptor.

The Consensus Structural Motif for the Sst$_1$-Selective SRIF Analogues. All of the sst$_1$-selective analogues with high-binding affinity studied here have either a β-turn (**1** to **4**) around D-Trp^{8}-IAmp^{9} or a γ-turn at IAmp^{9} (**5**). More importantly, they have similar spatial orientations/locations for some of the side chains, suggesting a role for these side chains in enhancing the

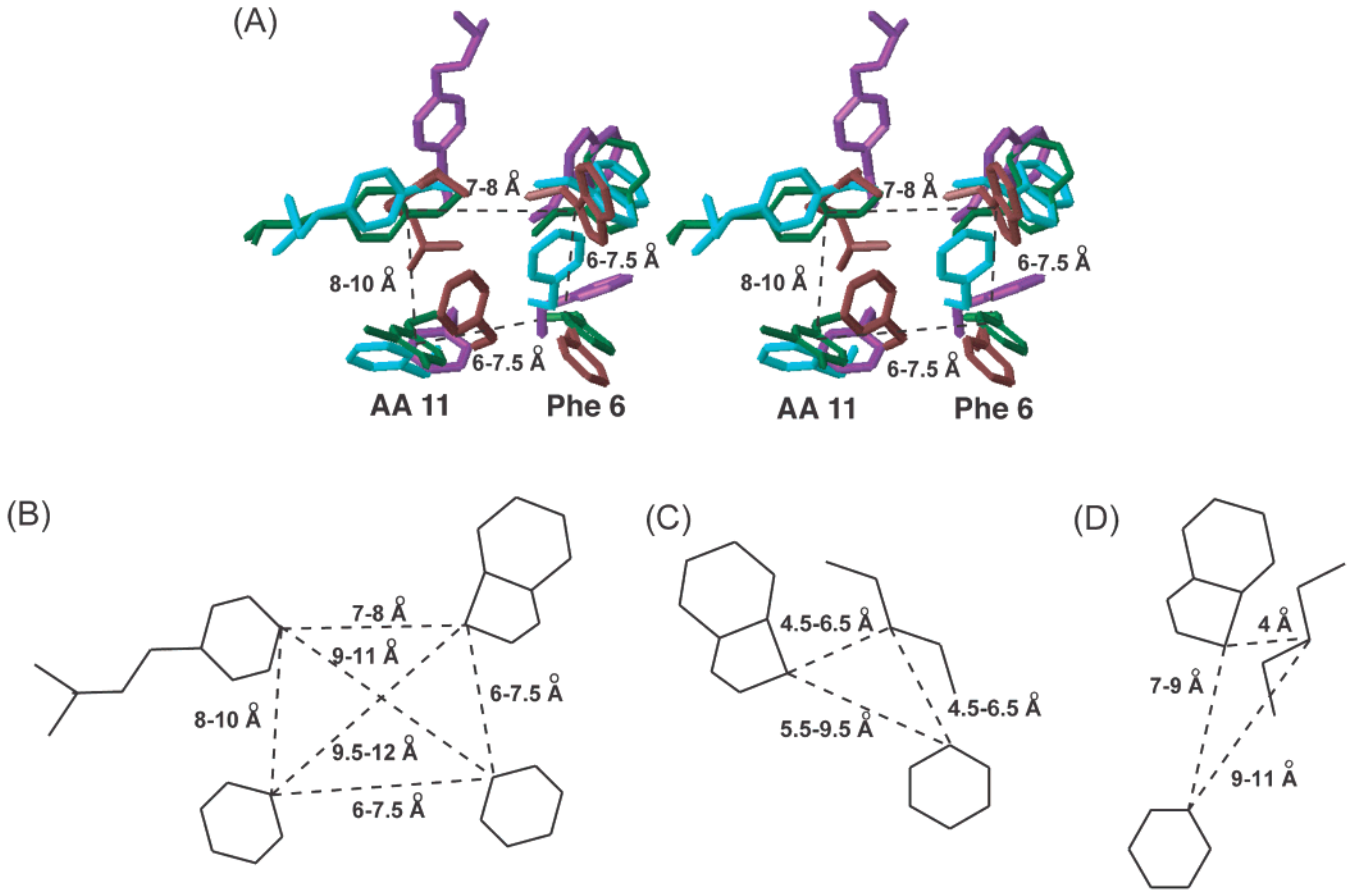

Figure 4. Consensus structural motif of sst_1-selective SRIF analogues. (A) Stereoview of the consensus structural motif for the sst_1-selective analogues **2** (violet), **3** (cyan), **4** (brown), and **5** (green). Only the side chains of D-Trp[8], IAmp[9], Phe[11], and Phe[6] or Phe[7] are shown. The distances between Cγ of D-Trp[8], IAmp[9], Phe[6], and Phe[11] are displayed. For each analogue, the conformer with the lowest target function is displayed. (B) Schematic drawing of the pharmacophore for the sst_1-selective analogues. (C) Schematic drawing of the pharmacophore for the sst_4-selective SRIF analogues.[23] (D) Schematic drawing of the pharmacophore for the sst_2/sst_5-selective SRIF analogues.[29]

binding affinity to sst_1 receptors as well as disrupting binding to other sst. Figure 2 shows the sst_1-selective analogues oriented individually, with specific color coding, highlighting the four side chains of interest, namely, the indole at position 8, D-Trp[8] (green), the aromatic-alkyl at position 9, IAmp[9] (blue), and the two aromatic rings at position 6 or 7 and 11 (yellow). Figure 4A shows the superposition of these four amino acids of **2** to **5** (as we shall see in the following, **1** and **6** have not been used in the definition of the consensus structure). Although the four structures superimposed contain different backbone conformations and are either monocyclic (**5**) or dicyclic (**2**−**4**), they all show a unique arrangement of the four side chains of residues: IAmp and D-Trp at the tip of the hairpin and the aromatic rings at position 6 or 7 and 11 on the front side of the peptide. This consensus structural motif, together with the binding affinities of the analogues (Table 1), clearly suggests that the arrangement of these four side chains Phe[6]/Phe[7], D-Trp[8], IAmp[9], and m-I-Tyr[11]/Phe[11] are important for high-affinity and selective binding to sst_1 (**5**).

The 3D structures determined for the four sst_1-selective SRIF analogues together with the data on bioactivity listed in Table 1 and preceding papers[1,2,13] enabled a detailed SAR study. In this consensus structural motif, the distances between the Cγ of residue Trp[8] and Cγ of Phe[6/7] is 6−7.5 Å, Cγ of residue Trp[8] and Cγ of IAmp[9] is 7−8 Å, Cγ of residue Trp[8] and Cγ of Phe/m-I-Tyr[11] is 9.5−12 Å, Cγ of residue IAmp[9] and Cγ of Phe[6/7] is 9−11 Å, Cγ of residue IAmp[9] and Cγ of Phe/m-I-Tyr[11] is 8−10 Å, and Cγ of Phe[6/7] and Phe/m-I-Tyr[11] is 6−7.5 Å. Higher binding affinity is obtained when the aromatic ring of Phe/m-I-Tyr[11] is in close proximity to the indole and the IAmp[9] side chains than otherwise. Conservative replacements of these residues do not change the binding affinities and receptor selectivity evidently.[1,2,13] However, IAmp replacement by Lys at position 9 enables the analogue to bind to all of the receptors, and hence a longer side chain at position 9 is important for selective binding to sst_1. Similarly, m-I-Tyr at position 11 almost exclusively increases the binding affinity by a factor of 2. Also the N-terminal carbamoylation increases the binding affinity by a factor of 2. The low-binding affinity of **1** can be explained by the misplacement of the aromatic rings at position 6 and 11, which are located on the backside of the peptide. Also in **6**, Phe[6] and m-I-Tyr[11] are located on the backside of the peptide. The higher binding affinity of this analogue compared to **1** is explained by the addition of m-I-Tyr and carbamoylation. Indeed, **6** without carbamoylation has a binding affinity lowered by a factor of 2 (data not shown).

Comparison of the Sst_1-Selective vs Sst_2/Sst_5- and Sst_4-Selective Pharmacophores. With the proposed consensus structural motif for the sst_1-selective

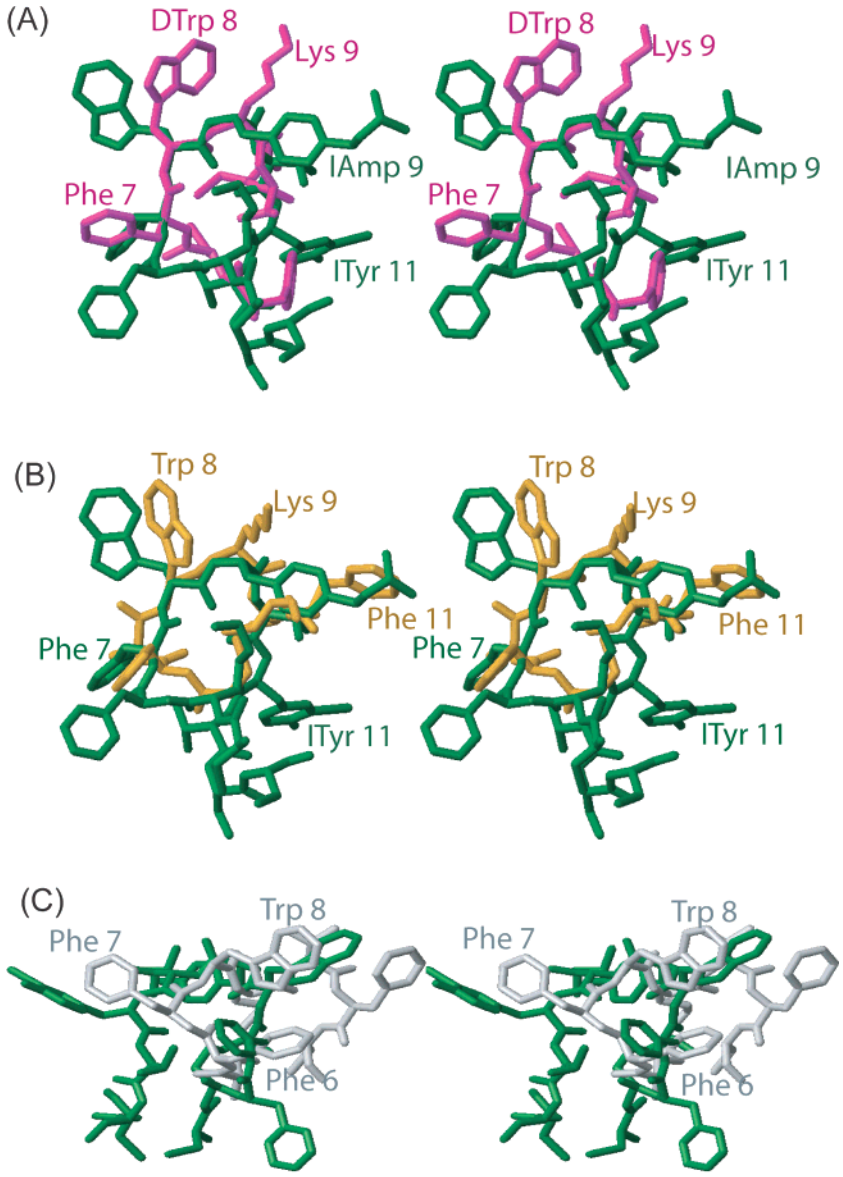

Figure 5. Comparison between the 3D structure of sst_1-selective with sst_2/sst_5-selective, sst_4-selective, and nonselective SRIF analogues. (A) Stereoview of the superposition of the 3D structure of the sst_1-selective analogue **5** (green) with the 3D structure of the sst_2/sst_5-selective octreotide (magenta).[29] It must be noted that m-I-Tyr^{11} is missing in octreotide which is important for selective binding to sst_1 receptors. Also, D-Trp-IAmp differs in their spatial orientation relative to the D-Trp-Lys pair. Phe^7 is also oriented on the backside of the peptide in sst_2/sst_5-selective pharmacophore. (B) Stereoview of the superposition of the 3D structure of the sst_1-selective analogue **5** (green) with the 3D structure of the sst_4-selective cyclo(3−14)H-Cys^3-Phe^6-Ala^7-Trp^8-Lys^9-Phe^{11}-Thr^{12}-Cys^{14}-OH (orange).[23] The sst_4 pharmacophore is completely different from sst_1 pharmacophore in the spatial orientation of Lys^9 and Phe^{11}. (C) Stereoview of the superposition of the 3D structure of the sst_1-selective **5** (green) with the 3D structure of the nonselective cyclo(3−14)H-Cys^3-Phe^6-Phe^7-Trp^8-Lys^9-Phe^{11}-Thr^{12}-Cys^{14}-OH, **7** (gray),[23] which binds with high affinity to all five receptors. This analogue has all the four side chains important for binding to sst_1 almost in the expected proximity and also the side chains important for sst_4.

SRIF analogues (Figure 4, parts A and B), a comparison of this motif with the proposed pharmacophore of sst_2/sst_5- and sst_4-selective analogues (Figures 4C and 4D) is carried out here. Goodman and co-workers illustrated that in SRIF analogues, which bind selectively to sst_2/sst_5, the side chains of D-Trp^8, Lys^9, and Phe^7 constitute the most essential elements necessary for binding.[28,29] In their pharmacophore model, the side chains of D-Trp^8 and Lys^9 were in close proximity of ∼4 Å (Cγ positions), but the side chain of Phe^7 was farther away from that of D-Trp^8 (7 to 9 Å), which varies from the sst_1 pharmacophore, wherein the phenylalanine (Phe$^{6/7}$) is in close proximity to D-Trp^8 (6−7.5 Å), while D-Trp^8 and IAmp^9 are at a proximity of 7−8 Å. This difference can easily be seen by superimposing the sst_1-selective **5** and the sst_2/sst_5-selective octreotide (Figure 5A).[29] In octreotide, Phe^7 is on the backside of the peptide, whereas in sst_1-selective **5**, the two aromatic side chains at position 7 and 11 are on the front side of the peptide. Furthermore, they differ in the position with respect to the indole ring at position 8 and from the side chain at position 9.

Recently our group has proposed a pharmacophore model of sst_4-selective analogues.[23] In this model, the side chains of D-Trp^8, Lys^9, and Phe^6 or Phe^{11} form the binding motif, with the aromatic ring in close proximity of 4.5 to 6.5 Å to Lys^9 and at a distance of 5.5−9.5 Å to the indole ring. This pharmacophore differs from that

of the sst_2/sst_5-selective analogues in the position of the phenylalanine ring[23] (Figure 4C). Comparing the sst_4 pharmacophore with that of sst_1 pharmacophore (Figure 5B) reveals that in the sst_4-selective analogue the aromatic ring of Phe^6 or Phe^{11} is close to the side chain of Lys^9 at the backside of the peptide and hence it is completely in a different position when compared with the m-I-Tyr/Phe^{11} of sst_1 selective pharmacophore, which are on the front side of the peptide (Figure 5B). Furthermore, the indole ring and the side chain of Lys are in close proximity in sst_4-selective analogues, whereas in the sst_1-selective pharmacophore they are farther apart. In summary, the sst_1 pharmacophore differs from sst_2 and sst_4 selective analogues by the side chain at position 9 and in the positions of the two aromatic rings at positions 6 or 7 and 11; they are on the front side of the peptide when interacting with sst_1 and are located on the backside when interacting with the sst_2/sst_5- and sst_4-selective analogues (Figures 4 and 5).

In our recent paper proposing the pharmacophore for the sst_4 receptor, we also solved the 3D structure of a highly active, but nonselective analogue **7** (Figure 5C, analogue **1**).[23] It is therefore interesting to determine whether this nonselective analogue contains the sst_1 pharmacophore as well. Clearly, structural interpretations of analogues with binding affinity to several receptors should be made with caution, because the binding to different receptors might involve an induced fit mechanism and therefore the structures determined might change upon binding. However, the intrinsic orientation of the side chains might already be prearranged. Indeed, we reported that the structure of **7**[23] contains the pharmacophore of sst_4 (Phe^{11} as part of the pharmacophore of sst_4). Interestingly, the side chains of Phe^6 and Phe^7 at the front side fit the proposed pharmacophore of sst_1-selective analogues, which is conserved in the 3D structure (Figure 5C). The relatively low binding affinity for sst_2 is reflected by a poor alignment of the sst_2/sst_5 pharmacophore in the 3D structure as well as the presence of Trp^8 instead of D-Trp. Overall, this observation further supports the proposed sst_1 pharmacophore.

Conclusions

The 3D conformations of six cyclic SRIF analogues having selective binding affinity to the sst_1 receptor have been studied in DMSO. In the analogues with high binding affinity (**2**−**5**), the relative spatial orientations of the side chains of D-Trp^8, $IAmp^9$, $Phe^{6/7}$, and Phe^{11}/m-I-Tyr^{11} are similar. These studies indicate that the backbone conformation forms a scaffold to orient the side chains of the essentially important residues, namely, tryptophan at position 8, aminoalkyl function at position 9, and two aromatic rings, in their respective positions for effective receptor−ligand binding. On the basis of the consensus structure, a pharmacophore has been proposed for sst_1-selective analogues consisting of these four side chains. This pharmacophore differs from that of sst_2/sst_5-selective analogues in the proximity between the side chains of IAmp and D-Trp as well as the aromatic side chains (Figure 4). It also differs from the pharmacophore of sst_4-selective analogues by one additional aromatic ring and also in the proximity between all of these side chains (Figure 5). The conformational study of the octapeptide analogues as well as of SRIF-14 that bind to all of the receptors also confirms the proposed model (data not shown). Furthermore, the model proposed also explains the selective binding of the nonpeptide analogues of SRIF agonists.[30−33] The structural elucidation of the sst_1-selective binding motif and the known motif for sst_4 and sst_2/sst_5-selective analogues support the detailed understanding of SRIF and its receptors and will have an important role in designing highly selective peptides as well as nonpeptide ligands of SRIF.

Experimental Section

Sample Preparation and NMR Experiments. Analogues were synthesized by the solid-phase approach either manually or on a CS-Bio peptide synthesizer model CS536.[1,2,7−9,13] NMR samples were prepared by dissolving 2.5 mg of the analogue in 0.5 mL of DMSO-d_6. The ^1H NMR spectra were recorded on a Bruker 700 MHz spectrometer operating at proton frequency of 700 MHz. Chemical shifts were measured using DMSO (δ = 2.49 ppm) as an internal standard. Also, the 1D spectra were acquired at temperatures between 300 and 323 K and were used to measure the temperature coefficients of the amide resonances. The 2D spectra were acquired at 298 K. Assignments of the various proton resonances have been carried out using total correlation spectroscopy (TOCSY),[34,35] double-quantum filtered spectroscopy (DQF-COSY),[36] and NOESY.[37−39] The TOCSY experiments employed the MLEV-17 spin-locking sequence suggested by Davis and Bax,[34] applied for a mixing time of 50 or 70 ms. The NOESY experiments were carried out with a mixing time of 100 ms. The TOCSY and NOESY spectra were acquired using 600 complex data points in the ω_1 dimension and 1024 complex data points in the ω_2 dimension with t_{1max} = 47 ms and a t_{2max} = 120 ms and were subsequently zero-filled to 1024 × 2048 before Fourier transformation. The DQF-COSY spectra were acquired with 1024 × 4096 data points and were zero-filled to 2048 × 4096 before Fourier transformation. The TOCSY, DQF-COSY, and NOESY spectra were acquired with 16, 16, and 64 scans, respectively, with a relaxation delay of 1 s. The signal from the residual water of the solvent was suppressed using presaturation during the relaxation delay as well as the mixing time. The TOCSY and NOESY data were multiplied by a 75° shifted sine function in both dimensions before Fourier transformation. All of the spectra were processed using the software PROSA (processing algorithms).[40] The spectra were analyzed using the software X-EASY in CARA.[41]

Structure Determination. The chemical shift assignment of the major conformer (the population of the minor conformer was <10%) was obtained by the standard procedure using DQF-COSY and TOCSY spectra for intraresidual assignment, and the NOESY spectrum was used for the sequential assignment.[42] The collection of structural restraints is based on the NOEs. Dihedral angle constraints were obtained from the intraresidual and sequential NOEs along with the macro GRIDSEARCH in the program CYANA (combined assignment and dynamics algorithm for NMR applications).[25] The calibration of NOE intensities versus $^1H-^1H$ distance restraints and appropriate pseudoatom corrections to the nonstereospecifically assigned methylene, methyl, and ring protons were performed using the program CYANA. On an average, approximately 150 NOE constraints and 20 angle constraints were utilized while calculating the conformers (Table 2). In analogues with the additional lactam bridge, the distance between the Cγ of the Glu^7 and the N_Z of Lys^9, Dbu^9, or L-$hhLys^9$ residues involved in the bridge was given as an additional distance restraint. A total of 100 conformers were initially generated by CYANA, and a bundle containing 20 CYANA conformers with the lowest target function values was utilized for further restrained energy minimization, using the CFF91 force field[43] with the energy criteria fit 0.1 kcal/(mol/Å)[44] in the program DISCOVER with steepest decent algo-

rithm[45] as described by Koerber et al.[44] The resulting energy-minimized bundle of 20 conformers was used as a basis for discussing the solution conformation of the different SRIF analogues. The structures were analyzed using the program MOLMOL.[46] The 3D structures of the analogues are deposited in the PDB database with codes 1XY4, 1XY5, 1XY6, 1XY8, 1XXZ, and 1XY9.

Acknowledgment. This work was supported in part by NIH Grant DK 59953. We thank Dr. W. Fisher and W. Low for mass spectrometric analyses, R. Kaiser, C. Miller, V. Eltschinger, and B. Waser for technical assistance in the synthesis and characterization of the peptides and biological testing. We are indebted to D. Doan for manuscript preparation. J.R. is The Dr. Frederik Paulsen Chair in Neurosciences Professor. We thank the H. and J. Weinberg Foundation, the H. N. and F. C. Berger Foundation, and the Auen Foundation for financial support. R.R. is the Pioneer Fund development Chair and a Pew Foundation scholar.

Supporting Information Available: Proton chemical shifts of analogues **1**−**6**. This material is available free of charge via the Internet at http://pubs.acs.org.

References

(1) Erchegyi, J.; Hoeger, C.; Low, W.; Hoyer, D.; Waser, B. et al. Somatostatin receptor 1 selective analogues: 2. N^{α}-methylated scan. *J. Med. Chem.* **2005,** *48***,** 507−514.
(2) Rivier, J.; Kirby, D.; Erchegyi, J.; Waser, B.; Eltschinger, V.; et al. Somatostatin receptor 1 selective analogues: 3. Dicyclic peptides. *J. Med. Chem.* **2005,** *48***,** 515−522.
(3) Reichlin, S. Somatostatin. *N. Engl. J. Med.* **1983***, 309*, 1495−1501.
(4) Reichlin, S. Somatostatin (second of two parts). *N. Engl. J. Med.* **1983***, 309*, 1556−1563.
(5) Delfs, J. R.; Dichter, M. A. Effects of somatostatin on mammalian cortical neurons in culture: physiological actions and unusual dose response characteristics. *J. Neurosci.* **1983***, 3*, 1176−1188.
(6) Iversen, L. L. Nonopioid neuropeptides in mammalian CNS. *Annu. Rev. Pharmacol. Toxicol.* **1983***, 23*, 1−27.
(7) Rivier, J.; Erchegyi, J.; Hoeger, C.; Miller, C.; Low, W. et al. Novel sst_4-selective somatostatin (SRIF) agonists. Part I: Lead identification using a betide scan. *J. Med. Chem.* **2003***, 46*, 5579−5586.
(8) Erchegyi, J.; Penke, B.; Simon, L.; Michaelson, S.; Wenger, S. et al. Novel sst_4-selective somatostatin (SRIF) agonists. Part II: Analogues with β-methyl-3-(2-naphthyl)-alanine substitutions at position 8. *J. Med. Chem.* **2003***, 46*, 5587−5596.
(9) Erchegyi, J.; Waser, B.; Schaer, J.-C.; Cescato, R.; Brazeau, J. F. et al. Novel sst_4-selective somatostatin (SRIF) agonists. Part III: Analogues amenable to radiolabeling. *J. Med. Chem.* **2003***, 46*, 5597−5605.
(10) Lewis, I.; Bauer, W.; Albert, R.; Chandramouli, N.; Pless, J. et al. A novel somatostatin mimic with broad somatotropin release inhibitory factor receptor binding and superior therapeutic potential. *J. Med. Chem.* **2003***, 46*, 2334−2344.
(11) Reubi, J. C.; Eisenwiener, K. P.; Rink, H.; Waser, B.; Macke, H. R. A new peptidic somatostatin agonist with high affinity to all five somatostatin receptors. *Eur. J. Pharmacol.* **2002***, 456*, 45−49.
(12) Janecka, A.; Zubrzycka, M.; Janecki, T. Review: Somatostatin analogs. *J. Pept. Res.* **2001***, 58*, 91−107.
(13) Rivier, J. E.; Hoeger, C.; Erchegyi, J.; Gulyas, J.; DeBoard, R. et al. Potent somatostatin undecapeptide agonists selective for somatostatin receptor 1 (sst1). *J. Med. Chem.* **2001***, 44*, 2238−2246.
(14) Reubi, J. C.; Schaer, J.-C.; Wenger, S.; Hoeger, C.; Erchegyi, J. et al. SST3-selective potent peptidic somatostatin receptor antagonists. *Proc. Natl. Acad. Sci. U.S.A.* **2000***, 97*, 13973−13978.
(15) Vale, W.; Rivier, C.; Brown, M.; Rivier, J. Pharmacology of TRF, LRF and somatostatin. *Hypothalamic Peptide Hormones and Pituitary Regulation: Advances in Experimental Medicine and Biology*; Plenum Press: New York, 1977; pp 123−156.
(16) Vale, W.; Rivier, J.; Ling, N.; Brown, M. Biologic and immunologic activities and applications of somatostatin analogs. *Metabolism* **1978***, 27*, 1391−1401.
(17) Veber, D. F.; Freidinger, R. M.; Perlow, D. S.; Paleveda, W. J., Jr.; Holly, F. W. et al. A potent cyclic hexapeptide analogue of somatostatin. *Nature* **1981***, 292*, 55−58.
(18) Pohl, E.; Heine, A.; Sheldrick, G. M.; Dauter, Z.; Wilson, K. S. et al. Structure of octreotide, a somatostatin analogue. *Acta Crystallogr.* **1995***, D51*, 48−59.
(19) Veber, D. F. Design and discovery in the development of peptide analogs. *Twelfth American Peptide Symposium*; Peptides: Chemistry and Biology: Cambridge, MA, June 16−21, 1991; pp 1−14.
(20) Falb, E.; Salitra, Y.; Yechezkel, T.; Bracha, M.; Litman, P. et al. A bicyclic and hsst2 selective somatostatin analogue: design, synthesis, conformational analysis and binding. *Bioorg. Med. Chem.* **2001***, 9*, 3255−3264.
(21) Jiang, S.; Gazal, S.; Gelerman, G.; Ziv, O.; Karpov, O. et al. A bioactive somatostatin analogue without a type II′ beta-turn: synthesis and conformational analysis in solution. *J. Pept. Sci.* **2001***, 7*, 521−528.
(22) Nattern, R.-H.; Moore, S. B.; Tran, T.-A.; Rueter, J. K.; Goodman, M. Synthesis, biological activities and conformational studies of somatostatin analogues. *Tetrahedron* **2000***, 56*, 9819−9831.
(23) Grace, C. R. R.; Erchegyi, J.; Koerber, S. C.; Reubi, J. C.; Rivier, J. et al. Novel sst_4-selective somatostatin (SRIF) agonists. Part IV: Three-dimensional consensus structure by NMR. *J. Med. Chem.* **2003***, 46*, 5606−5618.
(24) Nicolaou, K. C.; Salvino, J. M.; Raynor, K.; Pietranico, S.; Reisine, T. et al. Design and synthesis of a peptidomimetic employing β-D-glucose for scaffolding. *Peptides—Chemistry, Structure and Biology*; ESCOM Science Publishers B. V.: Leiden, The Netherlands, 1990; pp 881−884.
(25) Güntert, P.; Mumenthaler, C.; Wüthrich, K. Torsion angle dynamics for NMR structure calculation with the new program DYANA. *J. Mol. Biol.* **1997***, 273*, 283−298.
(26) Hagler, A. T.; Dauber, P.; Osguthorpe, D. J.; Hempel, J. C. Dynamics and conformational energetics of a peptide hormone: vasopressin. *Science* **1985***, 227*, 1309−1315.
(27) Melacini, G.; Zhu, Q.; Goodman, M. Multiconformational NMR analysis of sandostatin (octreotide): Equilibrium between β-sheet and partially helical structures. *Biochemistry* **1997***, 36*, 1233−1241.
(28) Huang, Z.; He, Y.; Raynor, K.; Tallent, M.; Reisine, T. et al. Side chain chiral methylated somatostatin analog synthesis and conformational analysis. *J. Am. Chem. Soc.* **1992***, 114*, 9390−9401.
(29) Melacini, G.; Zhu, Q.; Osapay, G.; Goodman, M. A refined model for the somatostatin pharmacophore: Conformational analysis of lanthionine-sandostatin analogs. *J. Med. Chem.* **1997***, 40*, 2252−2258.
(30) Ankersen, M.; Crider, M.; Liu, S.; Ho, B.; Andersen, H. S. et al. Discovery of a novel non-peptide somatostatin agonist with SST4 selectivity. *J. Am. Chem. Soc.* **1998***, 120*, 1368−1373.
(31) Liu, S.; Tang, C.; Ho, B.; Ankersen, M.; Stidsen, C. E. et al. Nonpeptide somatostatin agonists with sst_4 selectivity: Synthesis and structure−activity relationships of thioureas. *J. Med. Chem.* **1998***, 41*, 4693−4705.
(32) Rohrer, S. P.; Birzin, E. T.; Mosley, R. T.; Berk, S. C.; Hutchins, S. M. et al. Rapid identification of subtype-selective agonists of the somatostatin receptor through combinatorial chemistry. *Science* **1998***, 282*, 737−740.
(33) Prasad, V.; Birzin, E. T.; McVaugh, C. T.; Van Rijn, R. D.; Rohrer, S. P. et al. Effects of heterocyclic aromatic substituents on binding affinities at two distinct sites of somatostatin receptors. Correlation with the electrostatic potential of the substituents. *J. Med. Chem.* **2003***, 46*, 1858−1869.
(34) Davis, D. G.; Bax, A. Assignment of complex ^{1}H NMR spectra via two-dimensional homonuclear Hartmann−Hahn spectroscopy. *J. Am. Chem. Soc.* **1985***, 107*, 2820−2821.
(35) Braunschweiler, L.; Ernst, R. R. Coherence transfer by isotropic mixing: Application to proton correlation spectroscopy. *J. Magn. Reson.* **1983***, 53*, 521−528.
(36) Rance, M.; Sorensen, O. W.; Bodenhausen, B.; Wagner, G.; Ernst, R. R. et al. Improved spectral resolution in COSY1H NMR spectra of proteins via double quantum filtering. *Biochem. Biophys. Res. Commun.* **1983***, 117*, 479−485.
(37) Kumar, A.; Wagner, G.; Ernst, R. R.; Wüthrich, K. Buildup rates of the nuclear Overhauser effect measured by two-dimensional proton magnetic resonance spectroscopy: Implications for studies of protein conformation. *J. Am. Chem. Soc.* **1981***, 103*, 3654−3658.
(38) Macura, S.; Ernst, R. R. Elucidation of cross-relaxation in liquids by two-dimensional NMR spectroscopy. *Mol. Phys.* **1980***, 41*, 95−117.
(39) Macura, S.; Huang, Y.; Suter, D.; Ernst, R. R. Two-dimensional chemical exchange and cross-relaxation spectroscopy of coupled nuclear spins. *J. Magn. Reson.* **1981***, 43*, 259−281.

(40) Güntert, P.; Dotsch, V.; Wider, G.; Wüthrich, K. Processing of multidimensional NMR data with the new software PROSA. *J. Biolmol. NMR* **1992**, *2*, 619−629.
(41) Eccles, C.; Güntert, P.; Billeter, M.; Wüthrich, K. Efficient analysis of protein 2D NMR spectra using the software package EASY. *J. Biomol. NMR* **1991**, *1*, 111−130.
(42) Wüthrich, K. *NMR of Proteins and Nucleic Acids*; J. Wiley & Sons: New York, 1986.
(43) Maple, J. R.; Thacher, T. S.; Dinur, U.; Hagler, A. T. Biosym force field research results in new techniques for the extraction of inter- and intramolecular forces. *Chem. Design Auto. News* **1990**, *5*, 5−10.
(44) Koerber, S. C.; Rizo, J.; Struthers, R. S.; Rivier, J. E. Consensus bioactive conformation of cyclic GnRH antagonists defined by NMR and molecular modeling. *J. Med. Chem.* **2000**, *43*, 819−828.
(45) Hagler, A. T. Theoretical simulation of conformation, energetics and dynamics of peptides. *The Peptides: Analysis, Synthesis, Biology*; Academic Press: Orlando, FL, 1985; pp 213−299.
(46) Koradi, R.; Billeter, M. MOLMOL: a program for display and analysis of macromolecular structures. *PDB Newsletter* **1998**, *84*, 5−7.

JM049518U